CLEO CONF 99-12

Two-body B Meson Decays to η and η'–Observation of $B \to \eta K^*$

CLEO Collaboration

(August 5, 1999)

Abstract

In a sample of 19 million produced B mesons we have observed decays $B \to \eta K^*$, and improved our previous measurements of $B \to \eta' K$. The branching fractions we measure for these decay modes are $\mathcal{B}(B^+ \to \eta K^{*+}) = (27.3^{+9.6}_{-8.2} \pm 5.0) \times 10^{-6}$, $\mathcal{B}(B^0 \to \eta K^{*0}) = (13.8^{+5.5}_{-4.4} \pm 1.7) \times 10^{-6}$, $\mathcal{B}(B^+ \to \eta' K^+) = (80^{+10}_{-9} \pm 8) \times 10^{-6}$ and $\mathcal{B}(B^0 \to \eta' K^0) = (88^{+18}_{-16} \pm 9) \times 10^{-6}$. We have searched with comparable sensitivity for related nonstrange decays, and report upper limits for these rates. All quoted results are preliminary.

S. J. Richichi,[1] H. Severini,[1] P. Skubic,[1] A. Undrus,[1] M. Bishai,[2] S. Chen,[2] J. Fast,[2] J. W. Hinson,[2] J. Lee,[2] N. Menon,[2] D. H. Miller,[2] E. I. Shibata,[2] I. P. J. Shipsey,[2] Y. Kwon,[3,*] A.L. Lyon,[3] E. H. Thorndike,[3] C. P. Jessop,[4] K. Lingel,[4] H. Marsiske,[4] M. L. Perl,[4] V. Savinov,[4] D. Ugolini,[4] X. Zhou,[4] T. E. Coan,[5] V. Fadeyev,[5] I. Korolkov,[5] Y. Maravin,[5] I. Narsky,[5] R. Stroynowski,[5] J. Ye,[5] T. Wlodek,[5] M. Artuso,[6] R. Ayad,[6] E. Dambasuren,[6] S. Kopp,[6] G. Majumder,[6] G. C. Moneti,[6] R. Mountain,[6] S. Schuh,[6] T. Skwarnicki,[6] S. Stone,[6] A. Titov,[6] G. Viehhauser,[6] J.C. Wang,[6] A. Wolf,[6] J. Wu,[6] S. E. Csorna,[7] K. W. McLean,[7] S. Marka,[7] Z. Xu,[7] R. Godang,[8] K. Kinoshita,[8,†] I. C. Lai,[8] P. Pomianowski,[8] S. Schrenk,[8] G. Bonvicini,[9] D. Cinabro,[9] R. Greene,[9] L. P. Perera,[9] G. J. Zhou,[9] S. Chan,[10] G. Eigen,[10] E. Lipeles,[10] M. Schmidtler,[10] A. Shapiro,[10] W. M. Sun,[10] J. Urheim,[10] A. J. Weinstein,[10] F. Würthwein,[10] D. E. Jaffe,[11] G. Masek,[11] H. P. Paar,[11] E. M. Potter,[11] S. Prell,[11] V. Sharma,[11] D. M. Asner,[12] A. Eppich,[12] J. Gronberg,[12] T. S. Hill,[12] D. J. Lange,[12] R. J. Morrison,[12] T. K. Nelson,[12] J. D. Richman,[12] R. A. Briere,[13] B. H. Behrens,[14] W. T. Ford,[14] A. Gritsan,[14] H. Krieg,[14] J. Roy,[14] J. G. Smith,[14] J. P. Alexander,[15] R. Baker,[15] C. Bebek,[15] B. E. Berger,[15] K. Berkelman,[15] F. Blanc,[15] V. Boisvert,[15] D. G. Cassel,[15] M. Dickson,[15] P. S. Drell,[15] K. M. Ecklund,[15] R. Ehrlich,[15] A. D. Foland,[15] P. Gaidarev,[15] L. Gibbons,[15] B. Gittelman,[15] S. W. Gray,[15] D. L. Hartill,[15] B. K. Heltsley,[15] P. I. Hopman,[15] C. D. Jones,[15] D. L. Kreinick,[15] T. Lee,[15] Y. Liu,[15] T. O. Meyer,[15] N. B. Mistry,[15] C. R. Ng,[15] E. Nordberg,[15] J. R. Patterson,[15] D. Peterson,[15] D. Riley,[15] J. G. Thayer,[15] P. G. Thies,[15] B. Valant-Spaight,[15] A. Warburton,[15] P. Avery,[16] M. Lohner,[16] C. Prescott,[16] A. I. Rubiera,[16] J. Yelton,[16] J. Zheng,[16] G. Brandenburg,[17] A. Ershov,[17] Y. S. Gao,[17] D. Y.-J. Kim,[17] R. Wilson,[17] T. E. Browder,[18] Y. Li,[18] J. L. Rodriguez,[18] H. Yamamoto,[18] T. Bergfeld,[19] B. I. Eisenstein,[19] J. Ernst,[19] G. E. Gladding,[19] G. D. Gollin,[19] R. M. Hans,[19] E. Johnson,[19] I. Karliner,[19] M. A. Marsh,[19] M. Palmer,[19] C. Plager,[19] C. Sedlack,[19] M. Selen,[19] J. J. Thaler,[19] J. Williams,[19] K. W. Edwards,[20] R. Janicek,[21] P. M. Patel,[21] A. J. Sadoff,[22] R. Ammar,[23] P. Baringer,[23] A. Bean,[23] D. Besson,[23] R. Davis,[23] S. Kotov,[23] I. Kravchenko,[23] N. Kwak,[23] X. Zhao,[23] S. Anderson,[24] V. V. Frolov,[24] Y. Kubota,[24] S. J. Lee,[24] R. Mahapatra,[24] J. J. O'Neill,[24] R. Poling,[24] T. Riehle,[24] A. Smith,[24] S. Ahmed,[25] M. S. Alam,[25] S. B. Athar,[25] L. Jian,[25] L. Ling,[25] A. H. Mahmood,[25,‡] M. Saleem,[25] S. Timm,[25] F. Wappler,[25] A. Anastassov,[26] J. E. Duboscq,[26] K. K. Gan,[26] C. Gwon,[26] T. Hart,[26] K. Honscheid,[26] H. Kagan,[26] R. Kass,[26] J. Lorenc,[26] H. Schwarthoff,[26] E. von Toerne,[26] and M. M. Zoeller[26]

[1]University of Oklahoma, Norman, Oklahoma 73019
[2]Purdue University, West Lafayette, Indiana 47907
[3]University of Rochester, Rochester, New York 14627
[4]Stanford Linear Accelerator Center, Stanford University, Stanford, California 94309

[*]Permanent address: Yonsei University, Seoul 120-749, Korea.

[†]Permanent address: University of Cincinnati, Cincinnati OH 45221

[‡]Permanent address: University of Texas - Pan American, Edinburg TX 78539.

[5]Southern Methodist University, Dallas, Texas 75275
[6]Syracuse University, Syracuse, New York 13244
[7]Vanderbilt University, Nashville, Tennessee 37235
[8]Virginia Polytechnic Institute and State University, Blacksburg, Virginia 24061
[9]Wayne State University, Detroit, Michigan 48202
[10]California Institute of Technology, Pasadena, California 91125
[11]University of California, San Diego, La Jolla, California 92093
[12]University of California, Santa Barbara, California 93106
[13]Carnegie Mellon University, Pittsburgh, Pennsylvania 15213
[14]University of Colorado, Boulder, Colorado 80309-0390
[15]Cornell University, Ithaca, New York 14853
[16]University of Florida, Gainesville, Florida 32611
[17]Harvard University, Cambridge, Massachusetts 02138
[18]University of Hawaii at Manoa, Honolulu, Hawaii 96822
[19]University of Illinois, Urbana-Champaign, Illinois 61801
[20]Carleton University, Ottawa, Ontario, Canada K1S 5B6
and the Institute of Particle Physics, Canada
[21]McGill University, Montréal, Québec, Canada H3A 2T8
and the Institute of Particle Physics, Canada
[22]Ithaca College, Ithaca, New York 14850
[23]University of Kansas, Lawrence, Kansas 66045
[24]University of Minnesota, Minneapolis, Minnesota 55455
[25]State University of New York at Albany, Albany, New York 12222
[26]Ohio State University, Columbus, Ohio 43210

The dominant decay modes of B mesons involve the $\bar{b} \to \bar{c}$ quark transition with coupling to a W^+ boson. For many of these modes the decay amplitude may be described by a tree diagram in which the light quark (spectator) is bound in both the initial B meson and final charmed hadron via soft gluon exchange. With recent improvements in experimental sensitivity, less favored modes are becoming accessible. These include: $b \to u$ tree diagram transitions that are suppressed by the small Cabibbo-Kobayashi-Maskawa [1] (CKM) matrix element V_{ub}, such as $B \to \pi\ell\nu$ [2]; effective flavor changing neutral current (FCNC) decays $b \to s$ described by loop diagrams, such as the "electromagnetic penguin" $B \to K^*\gamma$ [3]; and decays to charmless hadrons such as $B \to K\pi$ [4–6]. The hadronic decays may be classified according to contributions to the amplitude from the several tree and penguin diagrams shown in Fig. 1 [7,8]. Some of these charmless hadronic decays offer prospects for the observation of CP violation, while others facilitate the quantitative understanding of the amplitudes that are essential to the interpretation of future CP measurements. For example, the decays $B \to \eta K$ and $B \to \eta' K$, with $B \to K\pi$, have been examined in this context [9,10].

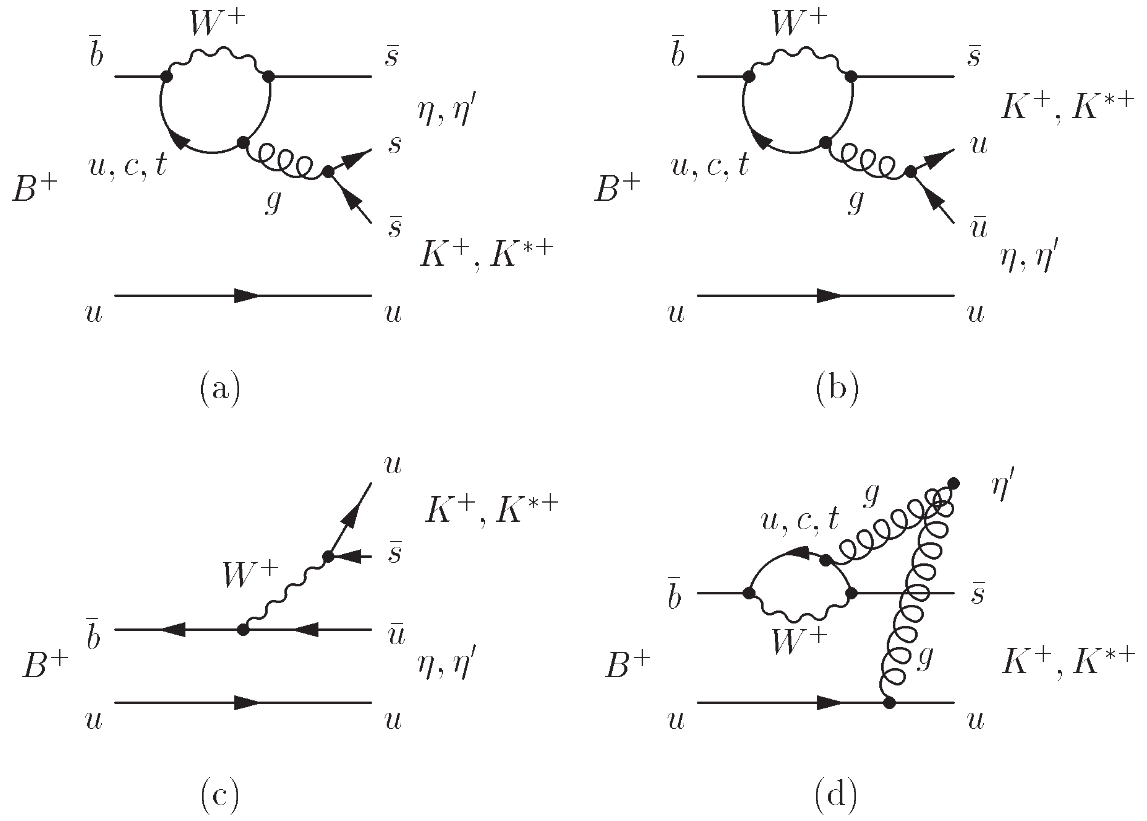

FIG. 1. Feynman diagrams describing the representative decays $B^+ \to \eta^{(\prime)} K^{(*)+}$: (a, b) internal penguins; (c) external tree; (d) flavor-singlet penguin.

In this paper we present results of several new experimental searches for B meson decays to two-body final states containing η and η' mesons. These $I = 0$ mesons are mixtures of flavor-SU(3) octet and singlet states, the latter being of particular interest because of its allowed formation through a pure (two or more) gluon intermediate state (Fig. 1 (d)).

The data were accumulated at the Cornell Electron-positron Storage Ring (CESR). The integrated luminosity was 9.13 fb^{-1} for the reaction $e^+e^- \to \Upsilon(4S) \to B\bar{B}$ (center-of-mass energy $E_{\rm cm} = 10.58$ GeV). This luminosity corresponds to the production of 9.6×10^6 charged and an approximately equal number of neutral B mesons. In addition we recorded 4.35 fb^{-1} of data with $E_{\rm cm}$ below the threshold for $B\bar{B}$ production to measure continuum processes. These constitute the complete data sample from the CLEO II and CLEO II.V experiments, and the measurements we report here succeed our earlier ones [11,12] from subsets of these data.

The CLEO II detector [13] emphasizes precision charged particle tracking, with specific ionization (dE/dx) measurement, and high resolution electromagnetic calorimetry based on CsI(Tl). Scintillators between the tracking chambers and calorimeter provide time-of-flight information which we use in conjuction with dE/dx for particle identification (PID). The CLEO II.V configuration differs in two respects: the addition of a silicon vertex detector; and replacement of the 50:50 argon:ethane gas in the main drift chamber with a 60:40 helium:propane mixture. From the raw data we reconstruct charged pions and kaons, photons (from π^0, η, and η' decays), and $\pi^+\pi^-$ pairs that intersect at a vertex displaced from the collision point ("vees", from $K^0_s \to \pi^+\pi^-$). Candidate B decay tracks must meet specifications on the number of drift chamber measurements, goodness of fit, and consistency with an origin at the primary or particular secondary vertex. Candidate photons must be isolated calorimeter clusters with a photon-like spatial distribution and energy deposition exceeding 30 MeV. We exclude photon pairs from extremely asymmetric η decays, requiring $|\cos\theta^*| < 0.97$, where θ^* is the meson center of mass decay angle relative to its flight direction. This cut rejects soft photon backgrounds and is tightened to 0.90 for K^*/ρ channels to veto $B \to K^*\gamma$ background. We reject charged tracks and photon pairs having momentum less than 100 MeV/c. The photon from candidate $\eta' \to \rho\gamma$ decays is generally required to have an energy greater than 200 MeV, though this requirement is relaxed to 100 MeV for channels with a K_S, which have low background.

We fit photon pairs and vees kinematically to the appropriate combined mass hypothesis to obtain the meson momentum vectors. Resolutions on the reconstructed masses prior to the constraint are about 5 – 10 MeV/c^2 (momentum dependent) for $\pi^0 \to \gamma\gamma$, 12 MeV/c^2 for $\eta \to \gamma\gamma$, and 3 MeV/c^2 for $K^0_s \to \pi^+\pi^-$. Information about expected signal distributions with the detector response comes from a detailed GEANT-based simulation of the CLEO detector [14] that reproduces the resolutions and efficiencies of data in a variety of benchmark processes. In particular, we have established the momentum and dE/dx resolutions in studies of $D^0 \to K^-\pi^+$ decays in a momentum range near 2.6 GeV/c.

Since the B mesons are formed nearly at rest, while the B daughters we observe are relatively light, the latter have momenta close to half of the beam energy (2.6 GeV/c). For this reason the final states are well separated from those involving heavier daughters, i.e., the dominant $b \to c$ decays. The principal signatures for the selected decay modes are consistency of the resonance decay invariant masses with the known masses and widths of those resonances, and consistency of the total final state with the B meson mass and energy. Because the beam energy E_b is better known than the reconstructed B meson energy E_B, we substitute the former in the B mass calculation: $M \equiv \sqrt{E_b^2 - \mathbf{p}_B^2}$, with $\mathbf{p}_B$ the reconstructed B momentum. We define also the variable $\Delta E \equiv E_B - E_b$. The measurement resolution on

M is 2.5 – 3 MeV/c^2, and on ΔE it is 25-50 MeV, depending on the apportionment of the energy among charged tracks and photons for each mode.

For vector-pseudoscalar decays of the B and the $\rho\gamma$ decay of the η' we gain further discrimination from the helicity variable $\mathcal{H}$ (cosine of the vector meson's rest frame two-body decay angle with respect to its flight direction), which reflects the spin alignment in the decay. The decay rate is proportional to $\mathcal{H}^2$ when the vector meson decays into two spinless daughters, and to $1 - \mathcal{H}^2$ for $\eta' \to \rho\gamma$. For modes in which one daughter is a single charged track we achieve statistical discrimination between kaons and pions by dE/dx. With S_K and S_π defined as the deviations from nominal energy loss for the indicated particle hypotheses measured in standard deviations, the separation $S_K - S_\pi$ is about 1.7 (2.0) at 2.6 GeV/c for the CLEO II (II.V) samples.

The main backgrounds arise from continuum quark production $e^+e^- \to q\bar{q}$. We discriminate against these jet-like events with several measures of the energy flow pattern. One is the angle θ_{BB} between the thrust axis (axis of maximum energy projection magnitude) of the candidate B and that of the rest of the event. For a fake B candidate selected from particles belonging to a $q\bar{q}$ event, those particles tend to align with the rest of the event, whereas the true B decays have a thrust axis that is largely uncorrelated with the tracks and showers from the decay of the partner B. We reject events with $|\cos\theta_{BB}| > 0.9$. In addition we use a multivariate discriminant $\mathcal{F}$ incorporating the energy deposition in nine cones concentric with the event thrust axis, and the angles of the thrust axis and $\mathbf{p}_B$ with respect to the e^+e^- beam direction [5]. We have checked the backgrounds from the favored B decay modes by simulation, finding their contributions to the modes in this study to be generally quite small. Where appropriate we include this component in the fits described below.

We set the selection criteria for mass, energy, and event shape variables so as to include sidebands about the expected signal peaks. To extract event yields we perform unbinned extended maximum likelihood fits to these data of a superposition of expected signal and background distributions:

$$\mathcal{L}(N_S, N_B) = \frac{e^{-(N_S+N_B)}}{N!} \prod_{i=1}^{N} \left[N_S \mathcal{P}_S(\vec{\beta}; \mathbf{x}_i) + N_B \mathcal{P}_B(\vec{\gamma}; \mathbf{x}_i) \right]. \tag{1}$$

Here $\mathcal{P}_S$ and $\mathcal{P}_B$ are the probability distribution functions (PDFs) for signal and continuum background, respectively. They are functions of observables $\mathbf{x}_i$ for event i, and of parameters $\vec{\beta}$ and $\vec{\gamma}$ (discussed below). The form of $\mathcal{L}$ reflects the underlying Poisson statistics obeyed by N_S and N_B, the (non-negative) numbers of signal and continuum background events, respectively. At the maximum of $\mathcal{L}$, $N_S + N_B$ is equal to the total number N of input events. Observables for each event include M, ΔE, $\mathcal{F}$, and (where applicable) resonance masses and $\mathcal{H}$. For these fits N ranges from ~ 100 to a few thousand.

For B^+ decays [16] that have a primary daughter charged hadron (generically h^+) that can be either π^+ or K^+ we fit both modes simultaneously, with $\mathcal{L}$ expanded so that the signal and background yields of both π^+ and K^+ are fit variables. In this case the PDFs depend also on the dE/dx observables S_π and S_K. The modes with a secondary vector decay (K^* or ρ) $\to h^+(\pi^-$ or $\pi^0)$ also require special treatment. For these modes the momentum spectrum of h^+ is bimodal because of the forward-backward peaked $\mathcal{H}$ distribution. We

TABLE I. Measurement results. The first column lists the final states, with secondary decay modes as subscripts. The vector modes with secondary decays to $h^+\pi^0$ or $h^+\pi^-$ are further distinguished with a subscript $(-)$ or $(+)$ depending on the value of $\mathcal{H}$ (see text). The remaining columns give event yield from the fit, reconstruction efficiency ϵ, total efficiency with secondary branching fractions $\mathcal{B}_s$, significance, and the resulting B decay branching fraction $\mathcal{B}$ with upper limit.

Final state	Fit events	ϵ(%)	$\epsilon\mathcal{B}_s$(%)	Signif. (σ)	$\mathcal{B}(10^{-6})$	90% UL(10^{-6})
$\eta'_{\eta\pi\pi}K^+$	$39.6^{+7.0}_{-6.4}$	27	4.7	13.4	88^{+16}_{-14}	–
$\eta'_{\rho\gamma}K^+$	61^{+11}_{-10}	29	8.7	10.1	72^{+13}_{-12}	–
$\eta'_{\eta\pi\pi}K^0$	$9.2^{+3.6}_{-2.9}$	24	1.4	7.7	67^{+26}_{-21}	–
$\eta'_{\rho\gamma}K^0$	$29.6^{+7.0}_{-6.2}$	28	2.9	8.9	105^{+25}_{-22}	–
$\eta'_{\eta\pi\pi}\pi^+$	$0.0^{+2.2}_{-0.0}$	28	4.7	0.0	$0.0^{+4.9}_{-0.0}$	13
$\eta'_{\rho\gamma}\pi^+$	$4.4^{+7.2}_{-4.4}$	30	9.0	0.8	$5.1^{+8.3}_{-5.1}$	21
$\eta_{\gamma\gamma}K^+$	$5.9^{+6.0}_{-4.6}$	45	17.5	1.4	$3.5^{+3.5}_{-2.7}$	10
$\eta_{3\pi}K^+$	$0.0^{+2.0}_{-0.0}$	29	6.6	0.0	$0.0^{+3.1}_{-0.0}$	9.4
$\eta_{\gamma\gamma}K^0$	$0.0^{+2.6}_{-0.0}$	38	5.1	0.0	$0.0^{+5.2}_{-0.0}$	12
$\eta_{3\pi}K^0$	$0.0^{+0.9}_{-0.0}$	25	1.9	0.0	$0.0^{+5.0}_{-0.0}$	23
$\eta_{\gamma\gamma}\pi^+$	$5.7^{+5.7}_{-4.6}$	46	18.2	1.3	$3.2^{+3.3}_{-2.6}$	9.2
$\eta_{3\pi}\pi^+$	$0.0^{+1.1}_{-0.0}$	30	6.8	0.0	$0.0^{+1.7}_{-0.0}$	7.0
$\eta_{\gamma\gamma}\pi^0$	$0.0^{+1.0}_{-0.0}$	35	13.7	0.0	$0.0^{+0.8}_{-0.0}$	3.9
$\eta_{3\pi}\pi^0$	$0.0^{+1.4}_{-0.0}$	20	4.6	0.0	$0.0^{+3.1}_{-0.0}$	11
$\eta_{\gamma\gamma}K^{*+}_{K^+\pi^0(-)}$	$9.2^{+4.4}_{-3.5}$	12	1.6	4.0	59^{+28}_{-23}	125
$\eta_{\gamma\gamma}K^{*+}_{K^+\pi^0(+)}$	$0.0^{+1.3}_{-0.0}$	9	1.2	0.0	0.0^{+12}_{-0}	53
$\eta_{3\pi}K^{*+}_{K^+\pi^0(-)}$	$1.1^{+1.7}_{-1.1}$	8	0.7	1.4	17^{+27}_{-17}	96
$\eta_{3\pi}K^{*+}_{K^+\pi^0(+)}$	$3.8^{+3.7}_{-2.5}$	6	0.5	1.9	80^{+77}_{-53}	269
$\eta_{\gamma\gamma}K^{*+}_{K^0\pi^+}$	$3.3^{+3.0}_{-2.1}$	24	2.2	2.1	16^{+14}_{-10}	44
$\eta_{3\pi}K^{*+}_{K^0\pi^+}$	$3.0^{+2.7}_{-1.9}$	17	0.9	2.1	34^{+30}_{-21}	98
$\eta_{\gamma\gamma}K^{*0}{}_{(-)}$	$6.9^{+3.9}_{-3.0}$	16	4.3	4.2	$16.7^{+9.4}_{-7.0}$	36
$\eta_{\gamma\gamma}K^{*0}{}_{(+)}$	$0.0^{+2.1}_{-0.0}$	15	4.0	0.0	$0.0^{+5.4}_{-0.0}$	17
$\eta_{3\pi}K^{*0}{}_{(-)}$	$4.7^{+3.1}_{-2.3}$	11	1.7	3.8	28^{+19}_{-14}	68
$\eta_{3\pi}K^{*0}{}_{(+)}$	$2.7^{+3.9}_{-2.7}$	10	1.6	1.0	18^{+25}_{-18}	69
$\eta_{\gamma\gamma}\rho^+{}_{(-)}$	$0.0^{+1.5}_{-0.0}$	12	4.8	0.0	$0.0^{+3.2}_{-0.0}$	14
$\eta_{\gamma\gamma}\rho^+{}_{(+)}$	$0.4^{+4.4}_{-0.4}$	9	3.6	0.1	1^{+12}_{-1}	31
$\eta_{3\pi}\rho^+{}_{(-)}$	$3.3^{+3.2}_{-2.1}$	8	1.9	2.1	18^{+17}_{-12}	58
$\eta_{3\pi}\rho^+{}_{(+)}$	$1.4^{+3.6}_{-1.4}$	6	1.4	0.6	10^{+26}_{-10}	118
$\eta_{\gamma\gamma}\rho^0$	$2.0^{+3.2}_{-2.4}$	26	10.3	1.1	$2.0^{+3.3}_{-2.0}$	10
$\eta_{3\pi}\rho^0$	$2.3^{+4.3}_{-2.3}$	18	4.2	0.7	6^{+11}_{-6}	28

select independent K^* and ρ samples to fit according to the sign of $\mathcal{H}$. Events with $\mathcal{H} < 0$ in our sign convention have low momentum h^+ and are unambiguously separated by kinematics combined with PID information from dE/dx measurements. For the events with $\mathcal{H} > 0$ the separation is less sharp, so we allow the yields for both h^+ hypotheses to float in the global likelihood fit and include the PID information. For K^{*0}/ρ^0 the choice of K or π is made on the basis of dE/dx and time-of-flight information.

The PDFs $\mathcal{P}_S$ and $\mathcal{P}_B$ are constructed as products of functions of the observables $\mathbf{x}_i$. The dependences of $\mathcal{P}_S$ on masses and energies are Gaussian, double Gaussian, or Breit-Wigner functions, whose means, widths, etc. appear as the parameters $\vec{\beta}$ in Eq. 1. The background PDF $\mathcal{P}_B$ contains signal-like peaking components in its resonance mass projections, to account for real resonances in the background, added to smooth components for combinatoric continuum. The smooth components are low-order polynomials, except that for M we use an empirical shape [15] that accounts for the phase space limit at $M = E_b$. The dependences of both $\mathcal{P}_S$ and $\mathcal{P}_B$ on $\mathcal{F}$, S_K, and S_π are bifurcated Gaussian functions. We obtain the parameters $\vec{\beta}$ of $\mathcal{P}_S$ from separate fits to simulated signal, and $\vec{\gamma}$ of $\mathcal{P}_B$ from fits to data in a sideband region of the ΔE – M plane. Where the Monte Carlo estimate of background from $\Upsilon(4S)$ production is non-negligible, we add a term with a free fit variable to account for this as well.

Results for all of the B decay chains appear in Table I. The row label subscripts denote secondary decays, including $\eta' \to \eta\pi^+\pi^-$ with $\eta \to \gamma\gamma$ ($\eta\pi\pi$), $\eta' \to \rho\gamma$ ($\rho\gamma$), and $\eta \to \pi^+\pi^-\pi^0$ (3π). For each mode the table gives the event yield from the likelihood fit, reconstruction efficiency, total efficiency, significance, branching fraction, and (where appropriate) 90% confidence level upper limit. Significance is defined as the number of standard deviations corresponding to the probability for a fluctuation from zero to our observed yield.

Where we have measured a given B decay mode in more than one secondary decay channel, we combine the samples by adding the $\chi^2 = -2\ln\mathcal{L}$ functions of branching fraction and extracting a value with errors or limit from the combined distribution. The limit is the value of $\mathcal{B}$ below which 90% of the integral of $\mathcal{L}$ lies. We summarize in Table II the results for these measurements, along with some earlier ones for related decays, and corresponding theoretical estimates [9,17–19]. We include systematic errors from uncertainties in the PDFs, i.e., in $\vec{\beta}$ and $\vec{\gamma}$, obtained from a Monte Carlo convolution of the likelihood function with Gaussian resolution functions for these parameters, including their most important correlations. This procedure changes the upper limit by less than 10% in most cases. We also include systematic errors for reconstruction efficiencies and selection requirements, and quote upper limits computed with efficiencies one standard deviation below nominal.

We have analyzed each of the decays also without use of the likelihood fit, employing more restrictive cuts in each of the variables to isolate the signals. The results are consistent with those quoted in the tables, but with larger errors (less restrictive limits) in most cases.

The positive signals we find in both charge states of $B \to \eta K^*$ are first observations: $\mathcal{B}(B^+ \to \eta K^{*+}) = (27.3^{+9.6}_{-8.2} \pm 5.0) \times 10^{-6}$ and $\mathcal{B}(B^0 \to \eta K^{*0}) = (13.8^{+5.5}_{-4.4} \pm 1.7) \times 10^{-6}$. (The first error quoted is statistical, the second systematic.) The significance is about 5 standard deviations for both, as can be seen in the likelihood functions from the fits shown in Fig. 2. For the $B \to \eta K^*$ decays we show also in Fig. 3 the projections of event distributions onto the M axis. The signals appear as peaks at the B meson mass of 5.28 GeV/c^2 in these plots, as well as in ΔE and the K^* mass.

TABLE II. Combined branching fractions. The fourth column gives our preliminary result, as central value followed by statistical and systematic error if significantly above zero, otherwise as a 90% confidence level upper limit. We quote estimates from various theoretical sources for comparison.

Decay mode	$\mathcal{B}_{\rm fit}(10^{-6})$	Signif. (σ)	$\mathcal{B}(10^{-6})$	Source	Theory $\mathcal{B}(10^{-6})$
$B^+ \to \eta' K^+$	$80^{+10}_{-9} \pm 8$	16.8	$80^{+10}_{-9} \pm 8$	This Exp.	7 – 65 [17,19]
$B^0 \to \eta' K^0$	$88^{+18}_{-16} \pm 9$	11.7	$88^{+18}_{-16} \pm 9$	This Exp.	9 – 59 [17,19]
$B^+ \to \eta' \pi^+$	$1.0^{+5.3}_{-1.0} \pm 0.1$	0.2	< 11	This Exp.	1 – 23 [17,19]
$B^0 \to \eta' \pi^0$			< 11	[11]	0.1 – 14 [17,19]
$B^+ \to \eta' K^{*+}$		1.2	< 87	[20]	0.1 – 3.7 [17,19]
$B^0 \to \eta' K^{*0}$		1.0	< 20	[20]	0.1 – 8.0 [17,19]
$B^+ \to \eta' \rho^+$			< 47	[11]	3 – 24 [17,19]
$B^0 \to \eta' \rho^0$			< 23	[11]	0.1 – 11 [17,19]
$B^+ \to \eta K^+$	$2.2^{+2.6}_{-2.2}$	1.0	< 7.1	This Exp.	0.2 – 5.0 [17,19]
$B^0 \to \eta K^0$	$0.0^{+3.0}_{-0.0}$	0.0	< 9.5	This Exp.	0.1 – 3.0 [17–19]
$B^+ \to \eta \pi^+$	$1.2^{+2.6}_{-1.2}$	0.6	< 6.0	This Exp.	1.9 – 7.4 [17–19]
$B^0 \to \eta \pi^0$	$0.0^{+0.7}_{-0.0}$	0.0	< 3.1	This Exp.	0.2 – 4.3 [17,19]
$B^+ \to \eta K^{*+}$	$27.3^{+9.6}_{-8.2} \pm 5.0$	4.8	$27.3^{+9.6}_{-8.2} \pm 5.0$	This Exp.	0.2 – 8.2 [17,19]
$B^0 \to \eta K^{*0}$	$13.8^{+5.5}_{-4.4} \pm 1.7$	5.1	$13.8^{+5.5}_{-4.4} \pm 1.7$	This Exp.	0.1 – 8.9 [17–19]
$B^+ \to \eta \rho^+$	$4.3^{+4.6}_{-3.4} \pm 0.7$	1.3	< 16	This Exp.	4 – 17 [17–19]
$B^0 \to \eta \rho^0$	$2.6^{+3.0}_{-2.4} \pm 0.3$	1.3	< 11	This Exp.	0.1 – 6.5 [17–19]

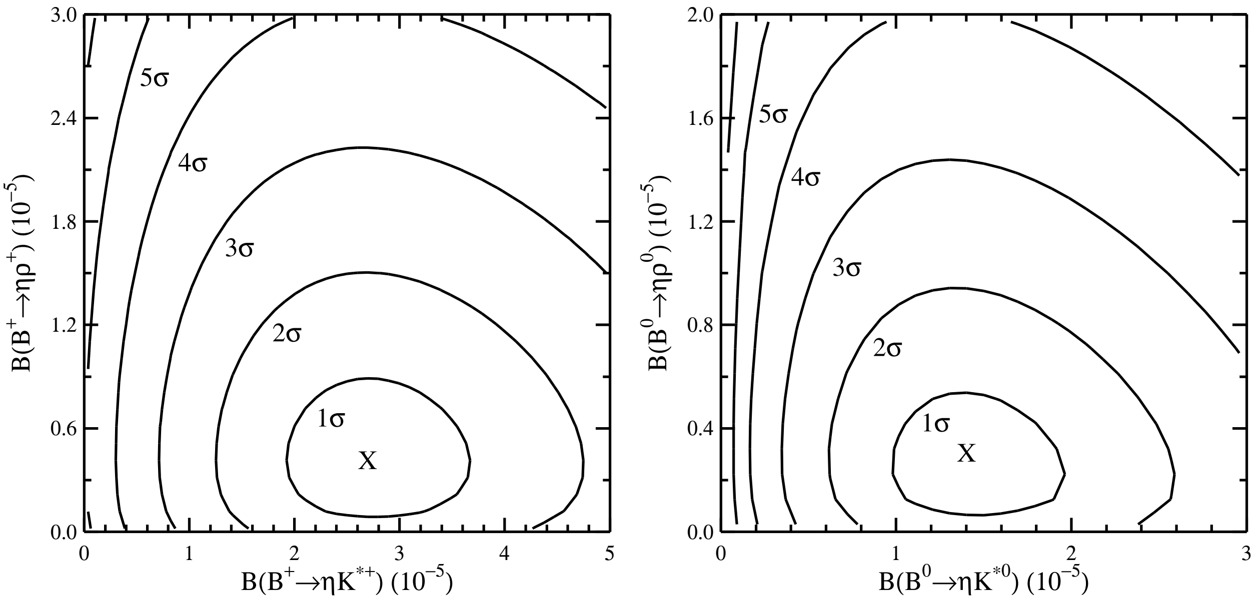

FIG. 2. Likelihood function contours for (a) $B^+ \to \eta\pi^0 h^+$; (b) $B^0 \to \eta\pi^- h^+$.

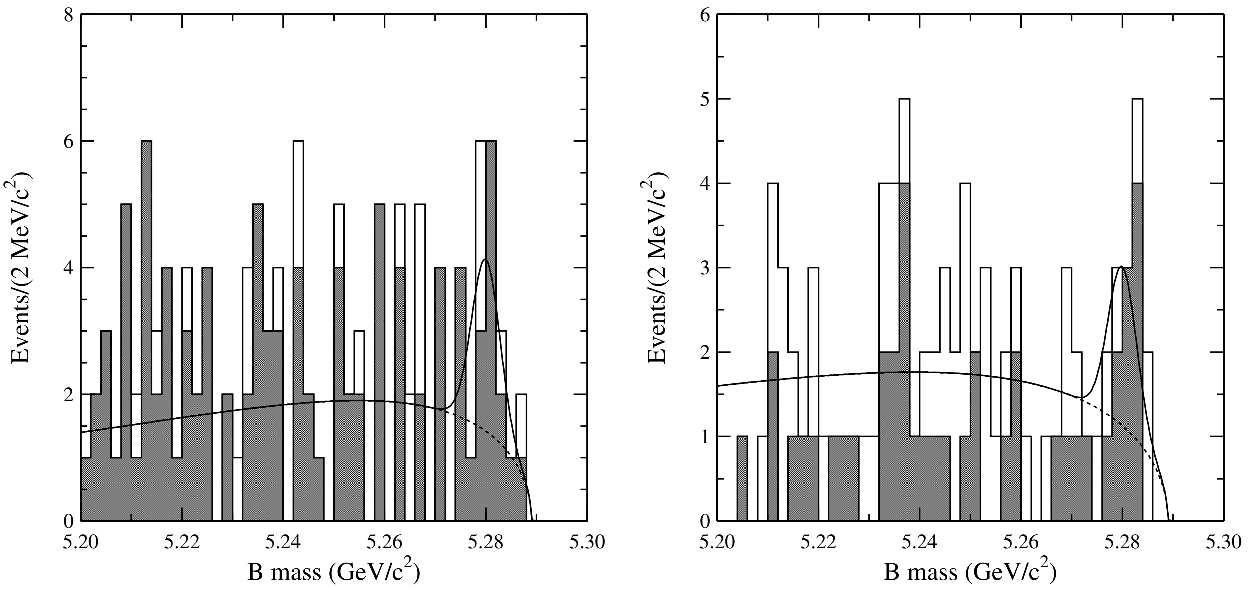

FIG. 3. Projections onto the variable M. Overlaid on each plot as smooth curves are the best fit functions (solid) and background components (dashed), calculated with the variables not shown restricted to the neighborhood of expected signal. The histograms show (a) $B^+ \to \eta K^{*+}$; (b) $B^0 \to \eta K^{*0}$. The unshaded histograms represent the $\mathcal{H} > 0$ K^* samples and the shaded is the rest.

With the full CLEO data sample we also improve our previous measurements [11,12] of $B \to \eta' K$. The new branching fractions are $\mathcal{B}(B^+ \to \eta' K^+) = (80^{+10}_{-9} \pm 8) \times 10^{-6}$ and $\mathcal{B}(B^0 \to \eta' K^0) = (88^{+18}_{-16} \pm 9) \times 10^{-6}$. The likelihood functions from the fits for $B \to \eta' h^+$ and $B^0 \to \eta' K^0$ are shown in Fig. 4. For these modes we show also in Fig. 5 the projections of event distributions onto the M axis.

The observed branching fractions for $B \to \eta' K$ and $B \to \eta K^*$, in combination with the upper limits for the other modes in Table II and with recent measurements of $B \to K\pi$, $\pi\pi$ [6], and $B \to \pi\rho$ [20], provide important constraints on the theoretical picture for these charmless hadronic decays.

The effective Hamiltonian calculations [8] commonly used to account for the charmless hadronic B decays contain uncertainties in form factors [21,22], light quark masses [22], and the QCD scale. They generally employ spectator and factorization [23] approximations, with unknown color octet terms arising from the expansion parameterized by an effective number of colors.

Two approaches, with many variations, to understanding these decay rates have been proposed. A large ratio of $(B \to \eta' K, \eta K^*)$ to $(B \to \eta K, \eta' K^*)$, consistent with our measurements, was predicted [24] in terms of interference of the two penguin diagrams in Fig. 1(a) and (b), constructive for $\eta' K$ and ηK^* and destructive for ηK and $\eta' K^*$. The argument is a bit more complicated for ηK^* than $\eta' K$, and there are probably cancellations that offset the enhancement. With independently estimated form factors the calculations tend to predict smaller rates than we observe.

The second class of ideas, which address particularly the large $\eta' K$ rate, take the η' to be

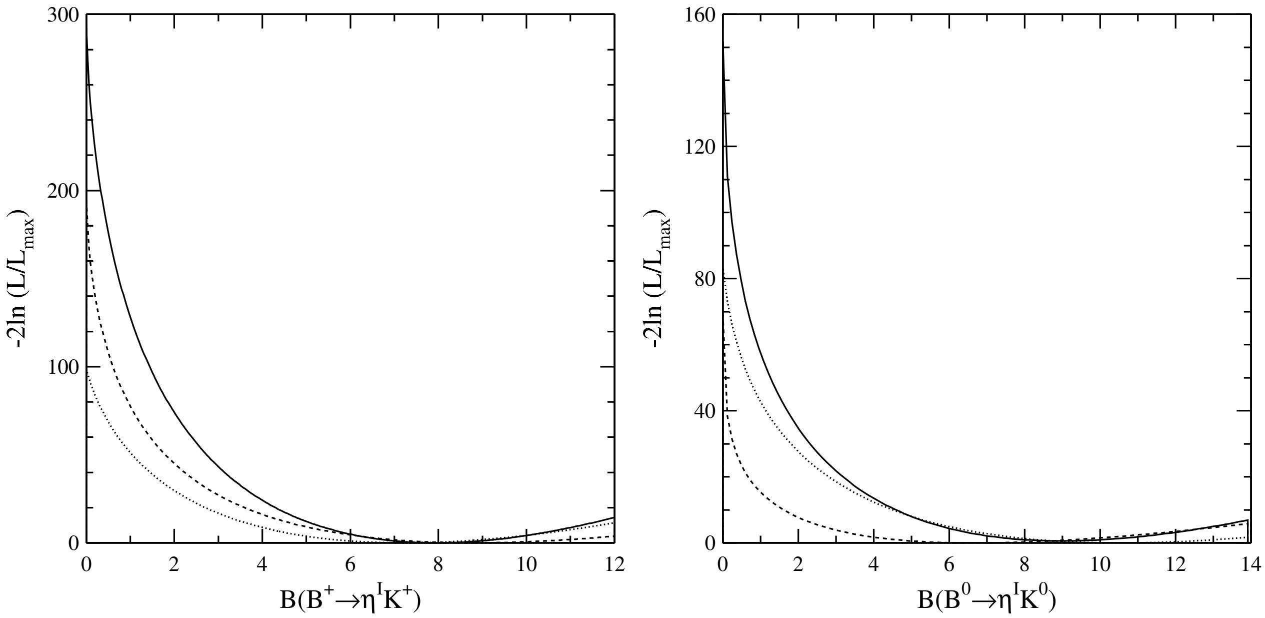

FIG. 4. The function $-2\ln\mathcal{L}/\mathcal{L}_{\max} = \chi^2 - \chi^2_{\min}$ for (a) $B^+ \to \eta' h^+$; (b) $B^0 \to \eta' K^0$. The dashed curve is for $\eta' \to \eta\pi^+\pi^-$ and the dotted curve for $\eta' \to \rho^0\gamma$.

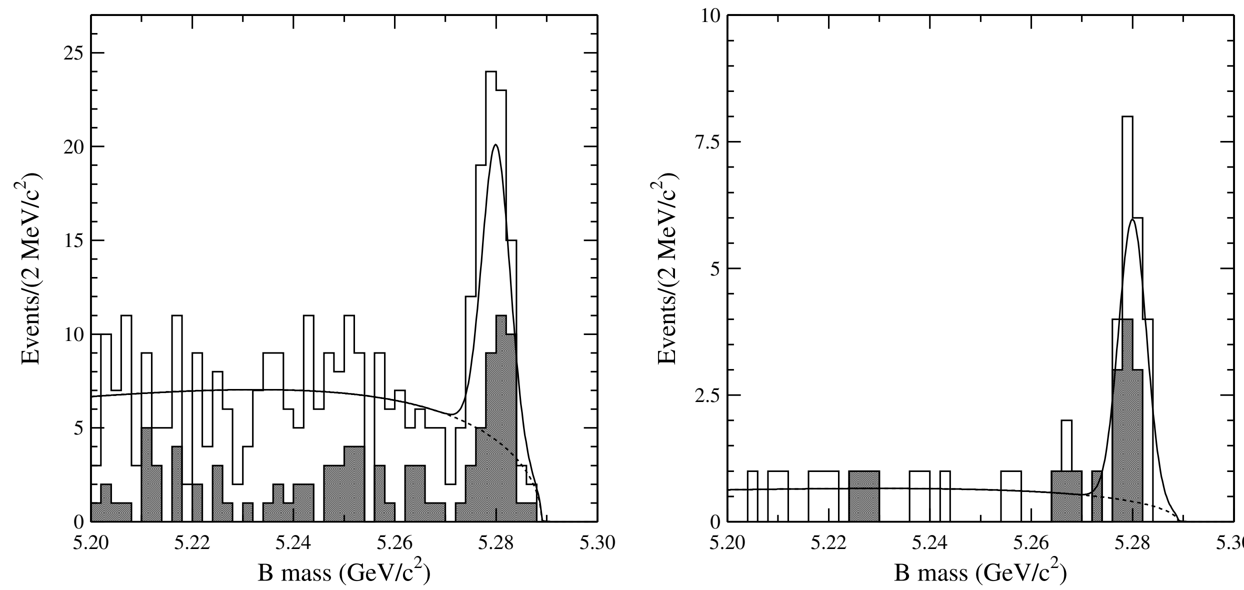

FIG. 5. Projections onto the variable M. Overlaid on each plot as smooth curves are the best fit functions (solid) and background components (dashed), calculated with the variables not shown restricted to the neighborhood of expected signal. The histograms show (a) $B^+ \to \eta' h^+$ with $\eta' \to \eta\pi\pi$ ($\eta \to 3\pi$, dark shaded), $\eta' \to \eta\pi\pi$ ($\eta \to \gamma\gamma$, light shaded), and $\eta' \to \rho\gamma$ (open); (b) $B^0 \to \eta' K^0$ with $\eta' \to \eta\pi\pi$ (shaded) and $\eta' \to \rho\gamma$ (open).

a special, poorly understood object with an anomaly contribution (Fig. 1 (d)) in constructive interference with the penguins [10,25,26]. This is related to speculations regarding the gluon [25] or $c\bar{c}$ content [27,28] of the η'. These are not equivalent; the anomaly term is a specific contribution which has been calculated (and shown to be insufficient to explain the data).

In combination, our ηK^* and $\eta' K$ observations suggest that perhaps the penguin interference mechanism is more important than current estimates give, with unexpectedly large form factors or some other mechanism favoring the penguin terms for both modes. The models that focus entirely on enhancement mechanisms for the η' appear to be insufficient to explain all of the data.

We thank George Hou and Hai-Yang Cheng for many useful discussions. We gratefully acknowledge the effort of the CESR staff in providing us with excellent luminosity and running conditions. J.R. Patterson and I.P.J. Shipsey thank the NYI program of the NSF, M. Selen thanks the PFF program of the NSF, M. Selen and H. Yamamoto thank the OJI program of DOE, J.R. Patterson, K. Honscheid, M. Selen and V. Sharma thank the A.P. Sloan Foundation, M. Selen and V. Sharma thank the Research Corporation, F. Blanc thanks the Swiss National Science Foundation, and H. Schwarthoff and E. von Toerne thank the Alexander von Humboldt Stiftung for support. This work was supported by the National Science Foundation, the U.S. Department of Energy, and the Natural Sciences and Engineering Research Council of Canada.

REFERENCES

[1] M. Kobayashi and T. Maskawa, Prog. Theor. Phys. **49**, 652 (1973).

[2] CLEO Collaboration, J. P. Alexander *et al.*, Phys. Rev. Lett. **77**, 5000 (1996).

[3] CLEO Collaboration, R. Ammar *et al.*, Phys. Rev. Lett. **71**, 674 (1993).

[4] CLEO Collaboration, M. Battle *et al.*, Phys. Rev. Lett. **71**, 3922 (1993).

[5] CLEO Collaboration, D. M. Asner *et al.*, Phys. Rev. D **53**, 1039 (1996).

[6] CLEO Collaboration, R. Godang *et al.*, Phys. Rev. Lett. **80**, 3456 (1998); CLEO Collaboration, paper contributed to this conference.

[7] See, for instance, Michael Gronau and Jonathan L. Rosner, Phys. Rev. D**53**, 2516 (1996); A. S. Dighe, Phys. Rev. D **54**, 2067 (1996); M. Gronau and J. L. Rosner, Phys. Rev. Lett. **76**, 1200 (1996).

[8] A. Ali and C. Greub, Phys. Rev. D **57**, 2996 (1998); A. Ali, G. Kramer, C.-D. Lu , Phys. Rev. D **59**, 014005 (1999); Y.-H. Chen, H.-Y. Cheng, B. Tseng, and K.-C. Yang, preprint hep-ph/9903453, March, 1999; N. G. Deshpande, B. Dutta, and S. Oh, Phys. Rev. D **57**, 5723 (1998); and references therein.

[9] G. Kramer, W. F. Palmer, and H. Simma, Zeit. Phys. C **66** 429 (1995).

[10] A. S. Dighe, M. Gronau, and J. L. Rosner, Phys. Rev. Lett. **79**, 4333 (1997); D. London and A. Soni, Phys. Lett. B **407**, 61 (1997).

[11] CLEO Collaboration, B. H. Behrens *et al.*, Phys. Rev. Lett. **80**, 3710 (1998).

[12] CLEO Collaboration, B. H. Behrens *et al.*, paper ICHEP98 860 contributed to the International Conference on High Energy Physics, Vancouver, BC (1998).

[13] CLEO Collaboration, Y. Kubota *et al.*, Nucl. Instrum. Methods Phys. Res., Sec. A **320**, 66 (1992).

[14] `GEANT 3.15`: R. Brun *et al.*, Report No. CERN DD/EE/84-1.

[15] With $x \equiv M/E_b$ and ξ a parameter to be fit, $f(x) \propto x\sqrt{1-x^2}\exp\left[-\xi(1-x^2)\right]$ (see H. Albrecht *et al.*, Phys. Lett. B **241**, 278 (1990); **254**, 288 (1991)).

[16] Inclusion of the charge conjugate states is implied throughout this paper.

[17] L.-L. Chau *et al.*, Phys. Rev. D **43**, 2176 (1991); erratum Phys. Rev. D **58**, 19902 (1998); reference 27.

[18] A. Deandrea *et al.*, Phys. Lett. B **318**, 549 (1993); **320**, 170 (1994).

[19] D. Du and L. Guo, Z. Phys. C **75**, 9 (1997).

[20] Y. Gao, W. Sun, F. Würthwein, talks presented at DPF99 and APS99; Yongsheng Gao and Frank Würthwein, hep-ex/9904008v2, Proceedings of APS/DPF 99, Los Angeles, CA (1999).

[21] A. Datta, X-G. He, and S. Pakvasa, Report No. UH-511-864-97 (1997).

[22] A. Kagan and A. Petrov, Report No. UCHEP-27 (1997).

[23] M. Bauer, B. Stech, and M. Wirbel, Z. Phys. C**43**, 103 (1987).

[24] H. J. Lipkin, Phys. Lett. B **254**, 247 (1991); this effect is incorporated in the predictions cited in Table II.

[25] David Atwood and Amarjit Soni, Phys. Lett. B **405**, 150 (1997).

[26] M. R. Ahmady, E. Kou, and A. Sugamoto, Report No. RIKEN-AF-NP-274 (1997); D. Du, C. S. Kim, and Y. Yang, Report No. BIHEP-TH/97-15 (1997).

[27] H-Y. Cheng and B. Tseng, Phys. Lett. B **415**, 263 (1997).

[28] M. Ciuchini *et al.*, Nucl. Phys. B **512**, 3 (1998); Igor Halperin and Ariel Zhitnitsky, Phys. Rev. D **56**, 7247 (1997).